Research Article | Vol. 8, No. 6 | 1 Jun 2018 | OPTICAL MATERIALS EXPRESS 1672
Optical Materials EXPRESS

Switching photonic nanostructures between cloaking and superscattering regimes using phase-change materials [Invited]

YIN HUANG,[1,*] YUECHENG SHEN,[2] CHANGJUN MIN,[3] AND GEORGIOS VERONIS[4,5]

[1]*Department of Optoelectrics Information Science and Engineering, School of Physics and Electronics, Central South University, Changsha, Hunan 410012, China*
[2]*Department of Medical Engineering, California Institute of Technology, Pasadena, CA 91125, USA*
[3]*Key Laboratory of Optoelectronic Devices and Systems of Ministry of Education and Guangdong Province, Shenzhen University, Shenzhen 518060, China*
[4]*School of Electrical Engineering and Computer Science, Louisiana State University, Baton Rouge, LA 70803, USA*
[5]*Center for Computation and Technology, Louisiana State University, Baton Rouge, LA 70803, USA*
[*]*yhuan15@csu.edu.cn*

Abstract: We show that phase-change materials can be used to switch photonic nanostructures between cloaking and superscattering regimes at mid-infrared wavelengths. More specifically, we investigate the scattering properties of subwavelength three-layer cylindrical structures in which the material in the outer shell is the phase-change material $Ge_2Sb_2Te_5$ (GST). We first show that, when GST is switched between its amorphous and crystalline phases, properly designed electrically small structures can switch between resonant scattering and cloaking invisibility regimes. The contrast ratio between the scattering cross sections of the cloaking invisibility and resonant scattering regimes reaches almost unity. We then also show that larger, moderately small cylindrical structures can be designed to switch between superscattering and cloaking invisibility regimes, when GST is switched between its crystalline and amorphous phases. The contrast ratio between the scattering cross sections of cloaking invisibility and superscattering regimes can be as high as ~ 93%. Our results could be potentially important for developing a new generation of compact reconfigurable optical devices.

OCIS codes: (260.0260) Physical optics; (290.5839) Scattering, invisibility; (050.6624) Subwavelength structures.

References and links

1. L. Novotny and B. Hecht, *Principles of Nano-Optics* (Cambridge University, 2006).
2. W. L. Barnes, A. Dereux, and T. W. Ebbesen, "Surface plasmon subwavelength optics," Nature **424**, 824–830 (2003).
3. S. Lal, S. Link, and N. J. Halas, "Nano-optics from sensing to waveguiding," Nat. Photonics **1**, 641–648 (2007).
4. M. I. Stockman, "Nanoplasmonics: past, present, and glimpse into future," Opt. Express **19**, 22029–22106 (2011).
5. Z. Yang, R. Jiang, X. Zhuo, Y. Xie, J. Wang, and H. Lin, "Dielectric nanoresonators for light manipulation," Phys. Rep. **701**, 1–50 (2017).
6. Y. Huang, G. Veronis, and C. Min, "Unidirectional reflectionless propagation in plasmonic waveguide-cavity systems at exceptional points," Opt. Express **23**, 29882–29895 (2015).
7. L. R. Hirsch, R. J. Stafford, J. A. Bankson, S. R. Sershen, B. Rivera, R. E. Price, J. D. Hazle, N. J. Halas, and J. L. West, "Nanoshell-mediated near-infrared thermal therapy of tumors under magnetic resonance guidance," Proc. Natl. Acad. Sci. USA **100**, 13549–13543 (2003).
8. J. B. Jackson and N. J. Halas, "Surface-enhanced Raman scattering on tunable plasmonic nanoparticle substrates," Proc. Natl. Acad. Sci. USA **101**, 17930–17935 (2004).
9. H. A. Atwater and A. Polman, "Plasmonics for improved photovoltaic devices," Nat. Mater. **9**, 205–213 (2010).
10. A. Alu and N. Engheta, "Cloaking a sensor," Phys. Rev. Lett. **102**, 233901 (2009).
11. P. Fan, U. K. Chettiar, L. Cao, F. Afshinmanesh, N. Engheta, and M. L. Brongersma, "An invisible metal-semiconductor photodetector," Nat. Photonics **6**, 380–385 (2012).
12. A. Alu and N. Engheta, "Cloaked near-field scanning optical microscope tip for noninvasive near-field imaging," Phys. Rev. Lett. **105**, 263906 (2010).

#328971 https://doi.org/10.1364/OME.8.001672
Journal © 2018 Received 23 Apr 2018; revised 21 May 2018; accepted 21 May 2018; published 30 May 2018

Optical Materials EXPRESS

13. A. Mirzaei, A. E. Miroshnichenko, I. V. Shadrivov, and Y. S. Kivshar, "Optical metacages," Phys. Rev. Lett. **115**, 215501 (2015).
14. A. Alu and N. Engheta, "Achieving transparency with plasmonic and metamaterial coatings," Phys. Rev. E **72**, 016623 (2005).
15. P. Chen, J, Soric, and A. Alu, "Invisibility and cloaking based on scattering cancellation," Adv. Mater. **24**, OP281–OP304 (2012).
16. A. Mirzaei, A. E. Miroshnichenko, I. V. Shadrivov, and Y. S. Kivshar, "All-dielectric multilayer cylindrical structures for invisibility cloaking," Sci. Rep. **5**, 9574 (2015).
17. S. Muhlig, M. Farhat, C. Rockstuhl, and F. Lederer, "Cloaking dielectric spherical objects by a shell of metallic nanoparticles," Phys. Rev. B **83**, 195116 (2011).
18. A. Monti, F. Bilotti, and A. Toscano, "Optical cloaking of cylindrical objects by using covers made of core-shell nanoparticles," Opt. Lett. **36**, 4479–4481 (2011).
19. Z. Ruan and S. Fan, "Superscattering of light from subwavelength nanostructures," Phys. Rev. Lett. **105**, 013901(2010).
20. Z. Ruan and S. Fan, "Design of subwavelength superscattering nanospheres," Appl. Phys. Lett. **98**, 043101(2011).
21. A. Mirzaei, A. E. Miroshnichenko, I. V. Shadrivov, and Y. S. Kivshar, "Superscattering of light optimized by a genetic algorithm," Appl. Phys. Lett. **105**, 011109 (2014).
22. Y. Huang and L. Gao, "Superscattering of light from core-shell nonlocal plasmonic nanoparticles," J. Phys. Chem. C **118**, 30170–30178 (2014).
23. X. Li, Q. Tan, B. Bai, and G. Jin, "Experimental demonstration of tunable directional excitation of surface plasmon polaritons with a subwavelength metallic double slit," Appl. Phys. Lett. **98**, 251109 (2011).
24. J. Lin, J. B. Mueller, Q. Wang, G. Yuan, N. Antoniou, X. Yuan, and F. Capasso, "Polarization-controlled tunable directional coupling of surface plasmon polaritons," Science **340**, 331–334 (2013).
25. S. Kim, H. Yun, K. Park, J. Hong, J. Yun, K. Lee, J. Kim, S. Jeong, S. Mun, J. Sung, Y. Lee, and B. Lee, "Active directional switching of surface plasmon polaritons using a phase transition material," Sci. Rep. **7**, 43723 (2017).
26. C. Argyropoulos, P. Chen, F. Monticone, G. D. Aguanno, and A. Alu, "Nonlinear plasmonic cloaks to realize giant all-optical scattering switching," Phys. Rev. Lett. **108**, 263905 (2012).
27. X. Chen, V. Sandoghdar, and M. Agio, "Coherent interaction of light with a metallic structure coupled to a single quantum emitter: from superabsorption to cloaking," Phys. Rev. Lett. **110**, 153605 (2013).
28. K. Shportko, S. Kremers, M. Woda, D. Lencer, J. Robertson, and M. Wuttig, "Resonant bonding in crystalline phase-change materials," Nat. Mater. **7**, 653–658 (2008).
29. M. Rude, V. Mkhitaryan, A. E. Cetin, T. A. Miller, A. Carrilero, S. Wall, F. J. Abajo, H. Altug, and V. Pruneri, "Ultrafast and broadband tuning of resonant optical nanostructures using phase-change materials," Adv. Optical Mater. **4**, 1060–1066 (2016).
30. D. Loke, T. H. Lee, W. J. Wang, L. P. Shi, R. Zhao, Y. C. Yeo, C. T. Chong, and S. R. Elliott, "Breaking the speed limits of phase-change memory," Science **336**, 1556–1569 (2012).
31. T. Hira, T. Homma, T. Uchiyama, K. Kuwamura, Y. Kihara, and T. Saiki, "All-optical switching of localized surface plasmon resonance in single gold nanosandwich using GeSbTe film as an active medium," Appl. Phys. Lett. **106,** 031105 (2015).
32. M. Wuttig and N. Yamada, "Phase-change materials for rewriteable data storage," Nat. Mater. **6**, 824–832 (2007).
33. M. H. R. Lankhorst, B. W. Ketelaarsand, and R. A. M. Wolters, "Low-cost and nanoscale non-volatile memory concept for future silicon chips," Nat. Mater. **4**, 347–352 (2005).
34. F. F. Schlich, P. Zalden, A. M. Lindenberg, and R. Spolenak, "Color switching with enhanced optical contrast in ultrathin phase change materials and semiconductors induced by femtosecond laser pulses," ACS Photonics **2**, 178–182 (2015).
35. M. Rude, R. E. Simpson, R. Quidant, V. Pruneri, and J. Renger, "Active control of surface plasmon waveguides with a phase change material," ACS Photonics **2**, 669–674 (2015).
36. Q. Wang, E. T. F. Rogers, B. Gholipour, C. Wang, G.Yuan, J. Teng, N. I. Zheludev, "Optically reconfigurable metasurfaces and photonic devices based on phase change materials," Nat. Photonics **10**, 60–65 (2016).
37. P. Li, X. Yang, T. W. W. Mab, J. Hanss, M. Lewin, A. U. Michel, M. Wuttig, and T. Taubner, "Reversible optical switching of highly confined phonon-polaritons with an ultrathin phase-change material," Nat. Mater. **15**, 870–876 (2016).
38. V. K. Mkhitaryan, D. S. Ghosh, M. Rude, J. Canet-Ferrer, R. A. Maniyara, K. K. Gopalan, and V. Pruneri, "Tunable complete optical absorption in multilayer structures including $Ge_2Sb_2Te_5$ without lithographic patterns," Adv. Optical Mater. **5**, 1600452 (2017).
39. S. Yoo, T. Gwon, T. Eom, S. Kim, and C. Hwang, "Multicolor changeable optical coating by adopting multiple layers of ultrathin phase change material film," ACS Photonics **3**, 1265–1270 (2016).
40. Y. Huang, Y. Shen, C. Min, and G. Veronis, "Switching of the direction of reflectionless light propagation at exceptional points in non-PT-symmetric structures using phase-change materials," Opt. Express **25**, 27283–27297 (2017).
41. C. F. Bohren and D. R. Huffman, *Absorption and Scattering of Light by Small Particles* (Wiley, 1998).
42. E. Thiessen, R. L. Heinisch, F. X. Bronold, and H. Fehske, "Surface mode hybridization in the optical response of core-shell particles," Phys. Rev. A **93**, 033827 (2016).
43. Y. Shen,1 L. V. Wang, and J. Shen, "Ultralong photonic nanojet formed by a two-layer dielectric microsphere," Opt.

Optical Materials EXPRESS

Lett. **39**, 4120–4123 (2014).
44. A. Mirzaei, I. V. Shadrivov, A. E. Miroshnichenko, and Y. S. Kivshar, "Cloaking and enhanced scattering of core-shell plasmonic nanowires," Opt. Express **21**, 10454–10459 (2013).
45. M. Razeghi and B. Nguyen, "Advances in mid-infrared detection and imaging: a key issues review," Rep. Prog. Phys. **77**, 082401 (2014).
46. C. Soci, A. Zhang, B. Xiang, S. A. Dayeh, D. P. R. Aplin, J. Park, X. Y. Bao, Y. H. Lo, and D. Wang, "ZnO nanowire UV photodetectors with high internal gain," Nano Lett. **7**, 1003–1009 (2007).
47. X. Liu, L. Gu, Q. Zhang, J. Wu, Y. Long, and Z. Fan, "All-printable band-edge modulated ZnO nanowire photodetectors with ultra-high detectivity," Nat. Commun. **5**, 4007 (2014).
48. R. Li, Z. Wei, F. Zhao, X. Gao, X. Fang, Y. Li, X. Wang, J. Tang, D. Fang, H. Wang, R. Chen, and X. Wang, "Investigation of localized and delocalized excitons in ZnO/ZnS core-shell heterostructured nanowires," Nanophotonics **7**, 1093–1100 (2017).
49. J. D. Jackson, *Classical Electrodynamics* (Wiley, 1998).
50. A. Alu, D. Rainwater, and A. Kerkhoff, "Plasmonic cloaking of cylinders: finite length, oblique illumination and cross-polarization coupling," New J. Phys. **12**, 103028 (2010).
51. F. Monticone, C. Argyropoulos, and A. Alu, "Multilayered plasmonic covers for comblike scattering response and optical tagging," Phys. Rev. Lett. **110**, 113901 (2013).
52. F. Monticone, C. Argyropoulos, and A. Alu, "Layered plasmonic cloaks to tailor the optical scattering at the nanoscale," Sci. Rep. **2**, 912 (2012).
53. M. G. Silveirinha, A. Alu, and N. Engheta, "Infrared and optical invisibility cloak with plasmonic implants based on scattering cancellation," Phys. Rev. B **78**, 075107 (2008).
54. M. E. Aryaee Panah, O. Takayama, S. V. Morozov, K. E. Kudryavtsev, E. S. Semenova, and A. V. Lavrinenko, "Highly doped InP as a low loss plasmonic material for mid-IR region," Opt. Express **24**, 29077–29088 (2016).
55. M. Farhat, S. Muhlig, C. Rockstuhl, and F. Lederer , "Scattering cancellation of the magnetic dipole field from macroscopic spheres," Opt. Express **20**, 13896–13906 (2012).
56. K. Kim, Y. No, S. Chang, J. Choi, and H. Park, "Invisible hyperbolic metamaterial nanotube at visible frequency," Sci. Rep. **5**, 16027 (2015).
57. C. Diaz-Avino, M. Naserpour, and C. J. Zapata-Rodriguez, "Optimization of multilayered nanotubes for maximal scattering cancellation," Opt. Express **24**, 18184–18196 (2016).
58. Y. Huang, C. Min, P. Dastmalchi, and G. Veronis, "Slow-light enhanced subwavelength plasmonic waveguide refractive index sensors," Opt. Express **11**, 14922–14936 (2015).
59. L. Zhang, R. Tu, and H. Dai, "Parallel core-shell metal-dielectric-semiconductor germanium nanowires for high-current surround-gate field-effect transistors," Nano Lett. **6**, 2785–2789 (2006).
60. P. R. Wiecha, A. Cuche, A. Arbouet, C. Girard, G. Francs, A. Lecestre, G. Larrieu, F. Fournel, V. Larrey, T. Baron, and V. Paillard, "Strongly directional scattering from dielectric nanowires," ACS Photonics **4**, 2036–2046 (2017).

1. Introduction

In recent years, investigating the interaction of light with subwavelength structures has attracted a lot of attention, since it could potentially lead to a new generation of photonic devices [1–6]. In particular, the capability to control the scattering of light and achieve invisibility cloaking of subwavelength structures is important for applications in biomedicine, photovoltaics, sensing, optical detection, and near-field imaging [7–13]. In the past few years, the use of plasmonic and dielectric multilayer coatings to drastically reduce the total scattering cross-section of deep subwavelength objects, and thus achieve invisibility cloaking based on scattering cancellation, has been explored [14–18]. In addition to cloaking, it has been demonstrated that subwavelength multilayer core-shell structures can lead to enhanced resonant scattering, so that the scattering cross sections of the original structures are greatly enhanced [19–22]. This phenomenon is commonly referred to as superscattering. Switching between the cloaking and enhanced scattering states could be essential for building compact optoelectronic devices, for reducing the size of optical systems, and for developing reconfigurable optical components [23–25]. Such switching between the enhanced scattering and invisibility cloaking regimes has been demonstrated using nonlinear materials [26] and quantum emitters [27]. An alternative way to achieve this switching could be through the use of materials with tunable optical properties, such as phase-change materials.

$Ge_2Sb_2Te_5$ (GST) is a phase-change material with an amorphous and a crystalline phase [28]. The covalently bonded amorphous phase of GST corresponds to a disordered material with

Optical Materials EXPRESS

short-range atomic order. In contrast, the resonantly bonded crystalline phase can be regarded as a semiconductor with orderly aligned atoms. Thus, the optical properties of amorphous GST (aGST) and crystalline GST (cGST) are significantly different. These two phases can be switched reversibly and rapidly by applying external electrical pulses, laser pulses or thermal annealing. Picosecond-order crystallization times have been reported for GST by femtosecond laser pulses [29, 30]. Amorphization of GeSbTe has been achieved on subpicosecond timescales with femtosecond laser pulse excitation [31]. In addition to being inexpensive and easy to use in device fabrication processes, GST retains its phase for years after removal of the external excitations. GST has been widely used for non-volatile, rewritable optical data storage devices and for electronic memories [32, 33]. Recently, it has been shown that GST could provide a versatile platform for the realization of optically reconfigurable active photonic devices due to its switchable dielectric properties [34–40].

In this paper, we investigate the scattering properties of a three-layer cylindrical structure with GST at the mid-infrared wavelength of 4 μm. We first consider an electrically small structure. We show that, when GST is switched between its amorphous and crystalline phases, the structure switches between resonant scattering and cloaking invisibility regimes. The contrast ratio between the scattering cross sections of the cloaking invisibility and resonant scattering regimes reaches almost unity. We then consider the case of a larger, moderately small cylindrical structure. In this scenario, we demonstrate that, when GST is switched between its crystalline and amorphous phases, the structure switches between superscattering and cloaking invisibility regimes. The contrast ratio between the scattering cross sections of cloaking invisibility and superscattering regimes can be as high as $\sim 93\%$. Although here we focus on two-dimensional infinitely long cylindrical structures, the proposed approach is rather general and can be applied to other optical structures.

The remainder of the paper is organized as follows. In Section 2, we employ the full-wave Mie-Lorenz mode-expansion method to describe the scattering properties of the proposed three-layer cylindrical structure. Using this theory, we analyze the switching between the cloaking invisibility and enhanced scattering regimes achieved for electrically small and larger, moderately small cylinders in Subsections 3.1 and 3.2, respectively. Finally, our conclusions are summarized in Section 4.

2. Theory

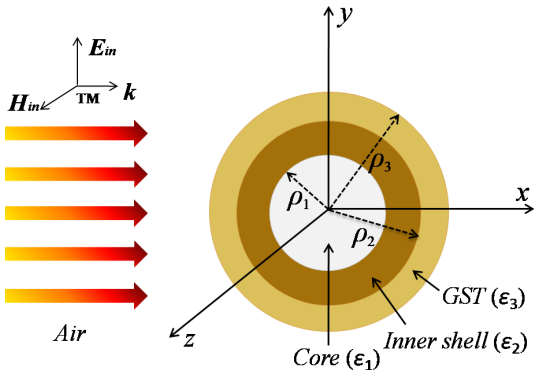

Fig. 1. Schematic of a three-layer core-shell cylindrical structure. The material in the outer shell is the phase-change material GST.

Our proposed three-layer cylindrical structure is normally illuminated by a TM plane wave propagating in the x direction with the magnetic field polarized along the cylinder (z) axis, as

Optical Materials EXPRESS

illustrated in Fig. 1. The material in the outer shell is the phase-change material GST. Based on the Mie-Lorenz mode-expansion method [41–43], the expansions for the incident fields are given by

$$\mathbf{H}_{in} = \sum_{n=-\infty}^{\infty} H_n \mathbf{N}_n^{(1)}, \tag{1}$$

$$\mathbf{E}_{in} = \frac{ik_0}{\omega\epsilon_0} \sum_{n=-\infty}^{\infty} H_n \mathbf{M}_n^{(1)}, \tag{2}$$

with expansion coefficients

$$H_n = \frac{H_0(-i)^n}{k_0}, \tag{3}$$

where H_0 is the strength of the incident magnetic field, k_0 is the wave number in free space, and ϵ_0 is the dielectric permittivity of free space. $\mathbf{M}_n$ and $\mathbf{N}_n$ are vector cylindrical harmonics of the n-th order [41]. The superscript (1) indicates that for the vector cylindrical harmonics the radial dependence of the fields is given by Bessel functions of the first kind J_n. The expansions of the fields in the core layer (Fig. 1) are

$$\mathbf{H}_1 = \sum_{n=-\infty}^{\infty} H_n [ic_n \mathbf{M}_n^{(1)} + d_n \mathbf{N}_n^{(1)}], \tag{4}$$

$$\mathbf{E}_1 = \frac{ik_1}{\omega\epsilon_1} \sum_{n=-\infty}^{\infty} H_n [ic_n \mathbf{N}_n^{(1)} + d_n \mathbf{M}_n^{(1)}], \tag{5}$$

where k_1 is the wave number in the core layer, and ϵ_1 is the dielectric permittivity of the material in the core. The expansions of the fields in the inner shell with dielectric permittivity ϵ_2 (Fig. 1) can be expressed as

$$\mathbf{H}_2 = \sum_{n=-\infty}^{\infty} H_n [ig_n \mathbf{M}_n^{(1)} + f_n \mathbf{N}_n^{(1)} + ip_n \mathbf{M}_n^{(2)} + q_n \mathbf{N}_n^{(2)}], \tag{6}$$

$$\mathbf{E}_2 = \frac{ik_2}{\omega\epsilon_2} \sum_{n=-\infty}^{\infty} H_n [ig_n \mathbf{N}_n^{(1)} + f_n \mathbf{M}_n^{(1)} + ip_n \mathbf{N}_n^{(2)} + q_n \mathbf{M}_n^{(2)}], \tag{7}$$

where k_2 is the wave number in the inner shell region. The superscript (2) indicates that for the vector cylindrical harmonics the radial dependence of the fields is given by Bessel functions of the second kind Y_n. Similarly, the expansions of the fields in the outer shell region can be written as

$$\mathbf{H}_3 = \sum_{n=-\infty}^{\infty} H_n [is_n \mathbf{M}_n^{(1)} + t_n \mathbf{N}_n^{(1)} + iw_n \mathbf{M}_n^{(2)} + v_n \mathbf{N}_n^{(2)}], \tag{8}$$

$$\mathbf{E}_3 = \frac{ik_3}{\omega\epsilon_3} \sum_{n=-\infty}^{\infty} H_n [is_n \mathbf{N}_n^{(1)} + t_n \mathbf{M}_n^{(1)} + iw_n \mathbf{N}_n^{(2)} + v_n \mathbf{M}_n^{(2)}], \tag{9}$$

where k_3 is the wave number in the outer shell, and ϵ_3 is the dielectric constant of GST. The scattered fields outside the three-layer cylindrical structure are given by

$$\mathbf{H}_s = \sum_{n=-\infty}^{\infty} H_n [ib_n \mathbf{M}_n^{(3)} + a_n \mathbf{N}_n^{(3)}], \tag{10}$$

$$\mathbf{E}_s = \frac{ik_0}{\omega\epsilon_0} \sum_{n=-\infty}^{\infty} H_n [ib_n \mathbf{N}_n^{(3)} + a_n \mathbf{M}_n^{(3)}]. \tag{11}$$

Optical Materials EXPRESS

The superscript (3) in the above equations indicates that for the vector cylindrical harmonics the radial dependence of the fields is given by Hankel functions of the first kind, H_n. By applying the boundary conditions at $\rho = \rho_j$, $j = 1, 2, 3$, we obtain the scattering coefficients a_n and b_n

$$a_n = 0, \tag{12}$$

$$b_n = \frac{U_n^{TM}}{U_n^{TM} + iV_n^{TM}}. \tag{13}$$

Note that the scattering coefficients a_n vanish when the plane wave is normally incident on the cylindrical structure [41]. In Eq. (13), U_n^{TM} and V_n^{TM} are given by

$$U_n^{TM} = \begin{vmatrix} J_n(k_1\rho_1) & J_n(k_2\rho_1) & Y_n(k_2\rho_1) & 0 & 0 & 0 \\ \frac{J_n'(k_1\rho_1)}{\eta_1} & \frac{J_n'(k_2\rho_1)}{\eta_2} & \frac{Y_n'(k_2\rho_1)}{\eta_2} & 0 & 0 & 0 \\ 0 & J_n(k_2\rho_2) & Y_n(k_2\rho_2) & J_n(k_3\rho_2) & Y_n(k_3\rho_2) & 0 \\ 0 & \frac{J_n'(k_2\rho_2)}{\eta_2} & \frac{Y_n'(k_2\rho_2)}{\eta_2} & \frac{J_n'(k_3\rho_2)}{\eta_3} & \frac{Y_n'(k_3\rho_2)}{\eta_3} & 0 \\ 0 & 0 & 0 & J_n(k_3\rho_3) & Y_n(k_3\rho_3) & J_n(k_0\rho_3) \\ 0 & 0 & 0 & \frac{J_n'(k_3\rho_3)}{\eta_3} & \frac{Y_n'(k_3\rho_3)}{\eta_3} & \frac{J_n'(k_0\rho_3)}{\eta_0} \end{vmatrix}, \tag{14}$$

and

$$V_n^{TM} = \begin{vmatrix} J_n(k_1\rho_1) & J_n(k_2\rho_1) & Y_n(k_2\rho_1) & 0 & 0 & 0 \\ \frac{J_n'(k_1\rho_1)}{\eta_1} & \frac{J_n'(k_2\rho_1)}{\eta_2} & \frac{Y_n'(k_2\rho_1)}{\eta_2} & 0 & 0 & 0 \\ 0 & J_n(k_2\rho_2) & Y_n(k_2\rho_2) & J_n(k_3\rho_2) & Y_n(k_3\rho_2) & 0 \\ 0 & \frac{J_n'(k_2\rho_2)}{\eta_2} & \frac{Y_n'(k_2\rho_2)}{\eta_2} & \frac{J_n'(k_3\rho_2)}{\eta_3} & \frac{Y_n'(k_3\rho_2)}{\eta_3} & 0 \\ 0 & 0 & 0 & J_n(k_3\rho_3) & Y_n(k_3\rho_3) & Y_n(k_0\rho_3) \\ 0 & 0 & 0 & \frac{J_n'(k_3\rho_3)}{\eta_3} & \frac{Y_n'(k_3\rho_3)}{\eta_3} & \frac{Y_n'(k_0\rho_3)}{\eta_0} \end{vmatrix}, \tag{15}$$

where $\eta_j = \sqrt{\frac{\epsilon_j}{\mu_j}}$, $j = 0, 1, 2, 3$. All materials are non-magnetic, so that $\mu_j = \mu_0$, $j = 1, 2, 3$. The total scattering cross section (SCS), defined as the ratio of the total scattered power to the intensity of the incident plane wave [12, 15, 41], is given by

$$\sigma = \frac{2\lambda_0}{\pi} \sum_{n=-\infty}^{\infty} |b_n|^2 = \frac{2\lambda_0}{\pi} \sigma_N, \tag{16}$$

where λ_0 is the free-space wavelength, and σ_N is the normalized scattering cross section (NSCS) [44]. Based on Eq. (13), $U_n^{TM} = 0$ leads to scattering suppression of the nth order multipole. Cloaking invisibility is achieved when all scattering coefficients b_n simultaneously approach zero. On the contrary, resonant scattering of the nth order multipole occurs when $V_n^{TM} = 0$, which provides an opportunity to dramatically enhance this scattering order. Based on electromagnetic duality, the scattering coefficients b_n for a normally incident TE excitation are zero, while $a_n = \frac{U_n^{TE}}{U_n^{TE} + iV_n^{TE}}$, where U_n^{TE} and V_n^{TE} can be readily obtained by replacing ϵ with μ in Eqs. (14) and (15), respectively [15, 41].

3. Results

In this section, we use the phase-change material GST in the three-layer cylindrical structure of Fig. 1, to switch this structure between cloaking and enhanced scattering regimes at the mid-infrared wavelength of $\lambda_0 = 4$ μm. Mid-infrared radiation in the 3−5 μm wavelength range can propagate through several materials without significant intensity attenuation. Because of this

Optical Materials EXPRESS

property, there is a wide range of potential military and civil applications in the mid-infrared wavelength regime [45]. For the material in the core of the three-layer cylindrical structure (Fig. 1) we choose zinc oxide (ZnO). Zinc oxide microwires and nanowires have great potential to be used in many commercial applications due to their low cost and simple fabrication process [46–48]. We use the commercial software COMSOL, which is based on the finite-element method, to numerically calculate the SCS of the proposed structures.

3.1. Electrically small cylindrical structures

We first consider electrically small cylindrical structures ($k_0\rho_3 \ll 1$). In this case, by using the asymptotic forms of the Bessel functions, the expressions in Eqs. (14) and (15) for $n \neq 0$ can be reduced to the following [49]

$$U_n^{TM} \simeq \frac{\pi(k_0\rho_3)^n}{4^n n!(n-1)!} \begin{vmatrix} 1 & 1 & -1 & 0 & 0 & 0 \\ \frac{1}{\epsilon_1} & \frac{1}{\epsilon_2} & \frac{1}{\epsilon_2} & 0 & 0 & 0 \\ 0 & (\frac{\rho_2}{\rho_1})^n & -(\frac{\rho_1}{\rho_2})^n & 1 & -1 & 0 \\ 0 & \frac{1}{\epsilon_2}(\frac{\rho_2}{\rho_1})^n & \frac{1}{\epsilon_2}(\frac{\rho_1}{\rho_2})^n & \frac{1}{\epsilon_3} & \frac{1}{\epsilon_3} & 0 \\ 0 & 0 & 0 & (\frac{\rho_3}{\rho_2})^n & -(\frac{\rho_2}{\rho_3})^n & 1 \\ 0 & 0 & 0 & \frac{1}{\epsilon_3}(\frac{\rho_3}{\rho_2})^n & \frac{1}{\epsilon_3}(\frac{\rho_2}{\rho_3})^n & \frac{1}{\epsilon_0} \end{vmatrix}, \tag{17}$$

and

$$V_n^{TM} \simeq (k_0\rho_3)^{-n} \begin{vmatrix} 1 & 1 & -1 & 0 & 0 & 0 \\ \frac{1}{\epsilon_1} & \frac{1}{\epsilon_2} & \frac{1}{\epsilon_2} & 0 & 0 & 0 \\ 0 & (\frac{\rho_2}{\rho_1})^n & -(\frac{\rho_1}{\rho_2})^n & 1 & -1 & 0 \\ 0 & \frac{1}{\epsilon_2}(\frac{\rho_2}{\rho_1})^n & \frac{1}{\epsilon_2}(\frac{\rho_1}{\rho_2})^n & \frac{1}{\epsilon_3} & \frac{1}{\epsilon_3} & 0 \\ 0 & 0 & 0 & (\frac{\rho_3}{\rho_2})^n & -(\frac{\rho_2}{\rho_3})^n & -1 \\ 0 & 0 & 0 & \frac{1}{\epsilon_3}(\frac{\rho_3}{\rho_2})^n & \frac{1}{\epsilon_3}(\frac{\rho_2}{\rho_3})^n & \frac{1}{\epsilon_0} \end{vmatrix}. \tag{18}$$

In addition, if the material in the core is dielectric and the structure is electrically small, the scattering cross section for TM excitation is dominated by the terms involving $b_{\pm 1}$, which are associated with dipolar scattering, and all other terms with $n \neq \pm 1$ are negligible [15, 50]. Note that $|b_n| = |b_{-n}|$ [41]. Thus, in this case, by setting $U_1^{TM} = 0$ in Eq. (17), we obtain the following condition to achieve invisibility cloaking

$$\phi_u = \gamma_2^2 = \frac{(\epsilon_3+\epsilon_0)[(\epsilon_2-\epsilon_1)(\epsilon_3+\epsilon_2)-(\epsilon_1+\epsilon_2)(\epsilon_2-\epsilon_3)\gamma_1^2]}{(\epsilon_0-\epsilon_3)[(\epsilon_1-\epsilon_2)(\epsilon_3-\epsilon_2)-(\epsilon_1+\epsilon_2)(\epsilon_2+\epsilon_3)\gamma_1^2]}, \tag{19}$$

where $\gamma_1 = \frac{\rho_2}{\rho_1}$ and $\gamma_2 = \frac{\rho_3}{\rho_2}$. Similarly, by setting $V_1^{TM} = 0$ in Eq. (18), we obtain the following condition to achieve enhanced scattering

$$\phi_v = \gamma_2^2 = \frac{(\epsilon_0-\epsilon_3)[(\epsilon_2-\epsilon_1)(\epsilon_3+\epsilon_2)-(\epsilon_1+\epsilon_2)(\epsilon_2-\epsilon_3)\gamma_1^2]}{(\epsilon_3+\epsilon_0)[(\epsilon_1-\epsilon_2)(\epsilon_3-\epsilon_2)-(\epsilon_1+\epsilon_2)(\epsilon_2+\epsilon_3)\gamma_1^2]}. \tag{20}$$

To realize switching of the three-layer cylindrical structure of Fig. 1 between cloaking and enhanced scattering regimes, requires $U_1^{TM} = 0$ when GST is in its crystalline phase with dielectric constant ϵ_{3c}, and also $V_1^{TM} = 0$ when GST is in its amorphous phase with dielectric constant ϵ_{3a}. In other words, when GST is in its crystalline phase with dielectric constant ϵ_{3c}, Eq. (19) should be satisfied, while, when GST is in its amorphous phase with dielectric constant ϵ_{3a}, Eq. (20) should be satisfied. Since the left hand sides of Eqs. (19) and (20) are equal, these two conditions can be simultaneously satisfied if $\phi_u(\epsilon_3 = \epsilon_{3c}) = \phi_v(\epsilon_3 = \epsilon_{3a})$. To achieve this, we

Optical Materials EXPRESS

optimize γ_1 and the dielectric constant of the inner shell ϵ_2, to satisfy the following relation at the wavelength of $\lambda_0 = 4\mu$m

$$|\phi_u(\epsilon_3 = \epsilon_{3c}) - \phi_v(\epsilon_3 = \epsilon_{3a})| = \left| \frac{(\epsilon_{3c} + \epsilon_0)[(\epsilon_2 - \epsilon_1)(\epsilon_{3c} + \epsilon_2) - (\epsilon_1 + \epsilon_2)(\epsilon_2 - \epsilon_{3c})\gamma_1^2]}{(\epsilon_0 - \epsilon_{3c})[(\epsilon_1 - \epsilon_2)(\epsilon_{3c} - \epsilon_2) - (\epsilon_1 + \epsilon_2)(\epsilon_2 + \epsilon_{3c})\gamma_1^2]} - \frac{(\epsilon_0 - \epsilon_{3a})[(\epsilon_2 - \epsilon_1)(\epsilon_{3a} + \epsilon_2) - (\epsilon_1 + \epsilon_2)(\epsilon_2 - \epsilon_{3a})\gamma_1^2]}{(\epsilon_{3a} + \epsilon_0)[(\epsilon_1 - \epsilon_2)(\epsilon_{3a} - \epsilon_2) - (\epsilon_1 + \epsilon_2)(\epsilon_2 + \epsilon_{3a})\gamma_1^2]} \right| = 0. \quad (21)$$

We use experimental data for the frequency-dependent dielectric constants of aGST and cGST [28]. The refractive indices of aGST and cGST are $\tilde{n}_{\text{aGST}} = 4.05$ and $\tilde{n}_{\text{cGST}} = 5.9 + 0.16j$, respectively, at $\lambda_0 = 4\mu$m [28,29]. Thus, at $\lambda_0 = 4\mu$m cGST is lossy, while aGST is lossless. The dielectric constant of zinc oxide, which is the material used in the core (Fig. 1), is $\epsilon_1 = 8.15$ at $\lambda_0 = 4\mu$m.

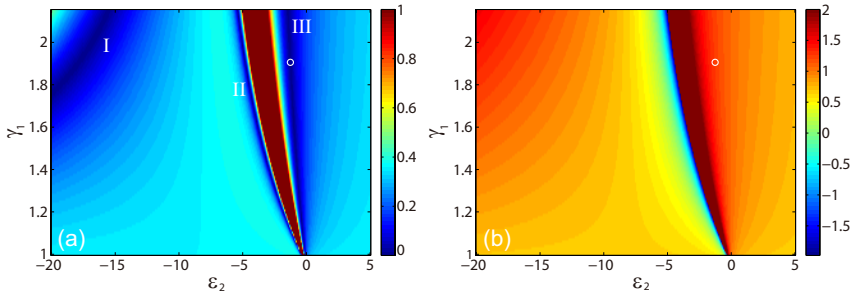

Fig. 2. (a) The quantity $|\phi_u(\epsilon_3 = \epsilon_{3c}) - \phi_v(\epsilon_3 = \epsilon_{3a})|$ as a function of $\gamma_1 = \frac{\rho_2}{\rho_1}$ and the dielectric constant of the inner shell ϵ_2 (Fig. 1). Results are shown for $\lambda_0 = 4\mu$m. Eq. (21) is satisfied at three regions in the γ_1-ϵ_2 space, marked as I, II, and III. The open circle corresponds to a point in region III. (b) The quantity $\gamma_2^2 = (\frac{\rho_3}{\rho_2})^2$ as a function of $\gamma_1 = \frac{\rho_2}{\rho_1}$ and the dielectric constant of the inner shell ϵ_2 (Fig. 1). Results are shown for $\lambda_0 = 4\mu$m.

We first neglect the loss of cGST at $\lambda_0 = 4\mu$m. In other words, we assume that $\epsilon_{3a} = 4.05^2 = 16.4$ and $\epsilon_{3c} = 5.9^2 = 34.81$. In Fig. 2(a), we show $|\phi_u(\epsilon_3 = \epsilon_{3c}) - \phi_v(\epsilon_3 = \epsilon_{3a})|$ as a function of $\gamma_1 = \frac{\rho_2}{\rho_1}$ and the dielectric constant of the inner shell ϵ_2. In Fig. 2(a) we observe three regions in the γ_1-ϵ_2 space (marked as I, II, and III) at which Eq. (21) is satisfied. However, since $\gamma_2^2 = (\frac{\rho_3}{\rho_2})^2$, only $\gamma_2^2 \geq 1$ corresponds to physical solutions. Figure 2(b) shows $\gamma_2^2 = (\frac{\rho_3}{\rho_2})^2$ as a function of $\gamma_1 = \frac{\rho_2}{\rho_1}$ and the dielectric constant of the inner shell ϵ_2. We observe that region II [Fig. 2(a)] does not correspond to physical solutions, since γ_2^2 is negative. On the other hand, regions I and III correspond to physical solutions. We consider a point in region III [indicated by an open circle in Figs. 2(a) and 2(b)] with $\gamma_1 = \frac{\rho_2}{\rho_1} = 1.9$, $\epsilon_2 = -1.25$, and $\gamma_2 = \frac{\rho_3}{\rho_2} = 1.1145$. Fig. 3(a) shows the NSCS σ_N corresponding to this point as a function of the dielectric constant of the outer shell ϵ_3 calculated with COMSOL. The radius of the ZnO core cylinder ρ_1 is set equal to 23 nm, so that the three-layer structure is electrically small ($k_0\rho_3 = k_0\rho_1\gamma_1\gamma_2 < 0.1$) [50]. We observe a peak ($\sigma_N \simeq 2|b_1|^2 = 1.9766$) and a dip ($\sigma_N \simeq 2|b_1|^2 = 1.01 \times 10^{-12}$) in the scattering cross section for $\epsilon_3 \simeq 16.4$ (aGST) and $\epsilon_3 \simeq 34.81$ (cGST), respectively. Thus, the simulation results confirm that for the optimized electrically small cylindrical structure of Fig. 1 switching between cloaking and enhanced scattering regimes can be realized at the mid-infrared wavelength of 4 μm by switching the phase-change material GST between its crystalline and amorphous phases. In Fig. 3(a), we also observe a resonance with asymmetric Fano-like shape at $\epsilon_3 = 0$. This is due to the strong interference between the cloaking and resonant scattering states within the same structure [51,52]. Based on Eqs. (19) and (20), the cloaking and resonant scattering conditions

Optical Materials EXPRESS

coincide with each other when $\epsilon_3 = 0$, and thus a degenerate cloaking-resonant state is formed. Figure 3(b) shows the NSCS σ_N as a function of $\gamma_1 = \frac{\rho_2}{\rho_1}$ for the optimized structure when the phase-change material GST is in its crystalline phase. Although the material loss in cGST affects the total scattering excursion, cloaking invisibility is still achieved ($\sigma_N = 4.2 \times 10^{-9}$) when $\gamma_1 = \frac{\rho_2}{\rho_1} = 1.9$ (red circles). The contrast ratio between the cloaking and resonant scattering states, defined as $\tau \equiv \left| \frac{\sigma_N|_{aGST} - \sigma_N|_{cGST}}{\sigma_N|_{aGST} + \sigma_N|_{cGST}} \right|$, is almost unity.

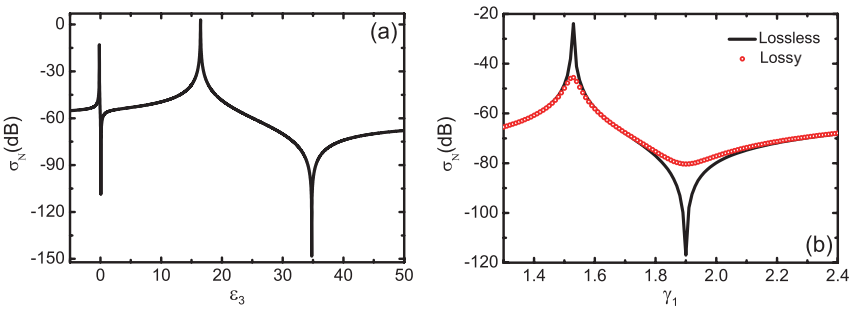

Fig. 3. (a) The NSCS σ_N as a function of the dielectric constant of the outer shell ϵ_3 for electrically small cylindrical structures as in Fig. 1. Results are shown for $\lambda_0 = 4\mu$m, $\rho_1 = 23$ nm, $\gamma_1 = \frac{\rho_2}{\rho_1} = 1.9$, $\gamma_2 = \frac{\rho_3}{\rho_2} = 1.1145$, and $\epsilon_2 = -1.25$. The material in the core is ZnO. (b) The NSCS σ_N as a function of $\gamma_1 = \frac{\rho_2}{\rho_1}$ when the phase change material GST in the outer shell is in its crystalline phase. The black line and red circles correspond to lossless and lossy cGST, respectively. All other parameters are as in Fig. 3(a).

The switching between cloaking and enhanced scattering regimes can be observed in the field distributions inside and outside the cylindrical structure for $\gamma_1 = \frac{\rho_2}{\rho_1} = 1.9$, $\gamma_2 = \frac{\rho_3}{\rho_2} = 1.1145$, $\rho_1 = 23$ nm, and $\epsilon_2 = -1.25$ (Fig. 4). When the plane wave is normally incident onto the optimized cylindrical structure with GST in its crystalline phase, the plane wave field distribution is not distorted at all by the presence of the structure [Figs. 4(a) and 4(b)]. On the other hand, when the plane wave is incident onto the optimized cylindrical structure with GST in its amorphous phase, the plane wave field distribution is severely distorted by the presence of the structure [Fig. 4(c)], and the incident wave excites a dipole mode supported by the structure [Fig. 4(d)]. In Fig. 2(a), we observe that in both regions I and III, which correspond to physical solutions, the dielectric permittivity of the inner shell ϵ_2 (Fig. 1) is negative. In general, an electrically small cylindrical structure exhibits a dipolar scattered field due to the electric dipole moment excited by the incident wave. The polarization vector in a shell with negative dielectric constant being antiparallel to those in other layers with positive dielectric constants may lead to the overall cancellation of dipole moment [14]. The dielectric permittivity of the inner shell has therefore to be negative to realize cloaking invisibility for our proposed optimized structure (Fig. 1) with GST in its crystalline phase. A material with dielectric constant ϵ being in the range $-10 < \epsilon < -0.5$ at infrared and visible frequencies can be formed by embedding silver implants in a dielectric host with positive dielectric constant [53]. In addition, there exist natural low loss plasmonic materials with the required negative dielectric permittivity at mid-infrared wavelengths, such as highly doped InP [54]. Its permittivity and plasmonic properties can be tuned through the carrier concentration [54]. In addition, we note that, even in the presence of loss in the inner shell, the contrast ratio is still close to unity [26]. As an example, we found that, for $\epsilon_2 = -1.25 + 0.1j$, the scattering cross section in the enhanced scattering regime is ~ 0.1, while the scattering cross section in the cloaking regime is $\sim 8.0 \times 10^{-7}$.

Optical Materials EXPRESS

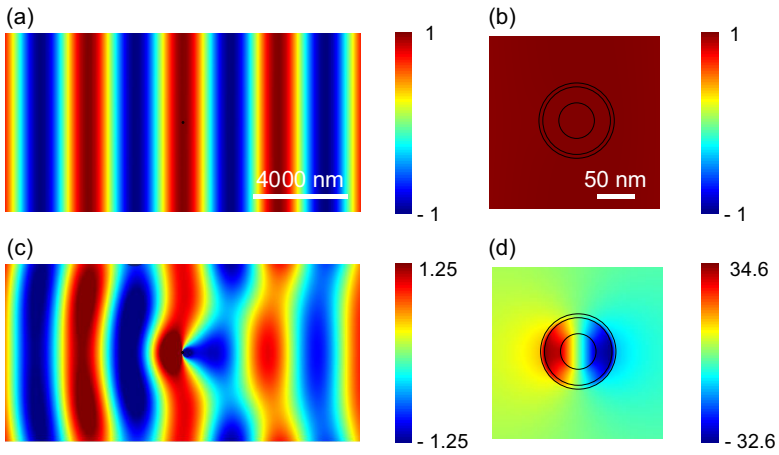

Fig. 4. (a) and (b) Magnetic field amplitude profiles for the optimized electrically small structure of Fig. 1 with GST in its crystalline phase at $\lambda_0 = 4$ μm, when a plane wave is normally incident from the left. All other parameters are as in Fig. 3(a). The fields are normalized with respect to the field amplitude of the incident plane wave. (c) and (d) Same as in (a) and (b) except that GST is in its amorphous phase.

3.2. *Moderately small cylindrical structures*

When the physical size of the cylindrical structure increases, other Mie scattering order contributions to the overall scattering cross section also need to be taken into account [55]. Thus, Eq. (21) can no longer be used to determine the optimized geometrical and material parameters of the structure in Fig. 1 for achieving switching between cloaking invisibility and enhanced scattering regimes, when GST is switched from its crystalline to its amorphous phase. In general, cloaking a moderately small structure through multiple scattering orders occurs when the numerators of the corresponding scattering coefficients [Eq. (13)] become zero at the same frequency. In addition, superscattering, which corresponds to the scattering cross section of a moderately small structure being significantly enhanced, occurs when overlap of at least two different scattering resonance modes is achieved at the same frequency [19,20,44]. In this subsection, the radius of the core layer is set equal to 480 nm which is approximately 10 times larger than the radius of the optimized electrically small three-layer cylindrical structure in Subsection 3.1. In addition, the material of the inner shell is chosen to be TiO_2 with dielectric constant which can be approximated by the following Sellmeier dispersion equation [56,57]

$$\epsilon_{TiO_2} = \epsilon_2 = 5.193 + \frac{0.244}{\lambda_0^2 - 0.0803}, \tag{22}$$

where the wavelength λ_0 is in units of micrometers. Thus, the dielectric constant of TiO_2 at the operating wavelength of $\lambda_0 = 4$ μm is ~ 5.2. To realize switching between cloaking and superscattering regimes for the moderately small cylindrical structure of Fig. 1, we now use Eqs. (14) and (15) (Section 2). More specifically, we optimize $\gamma_1 = \frac{\rho_2}{\rho_1}$ and $\gamma_2 = \frac{\rho_3}{\rho_2}$ (Fig. 1) to make the NSCS of the structure [Eq. (16)] as large as possible when GST is in its csystalline phase, and as small as possible when GST is in its amorphous phase at the wavelength of $\lambda_0 = 4$ μm.

In Fig. 5, we show the NSCS σ_N of the proposed moderately small core-shell cylindrical structure for different scattering orders as a function of $\gamma_1 = \frac{\rho_2}{\rho_1}$ and $\gamma_2 = \frac{\rho_3}{\rho_2}$, when GST is in its crystalline phase [Figs. 5(a)-5(d)], and its amorphous phase [Figs. 5(e)-5(h)] at the wavelength of $\lambda_0 = 4$ μm. For the range of parameters shown, the amplitudes of the higher order coefficients $|b_n|$ are negligible for $|n| > 3$. When the phase-change material GST is in its crystalline phase,

Optical Materials EXPRESS

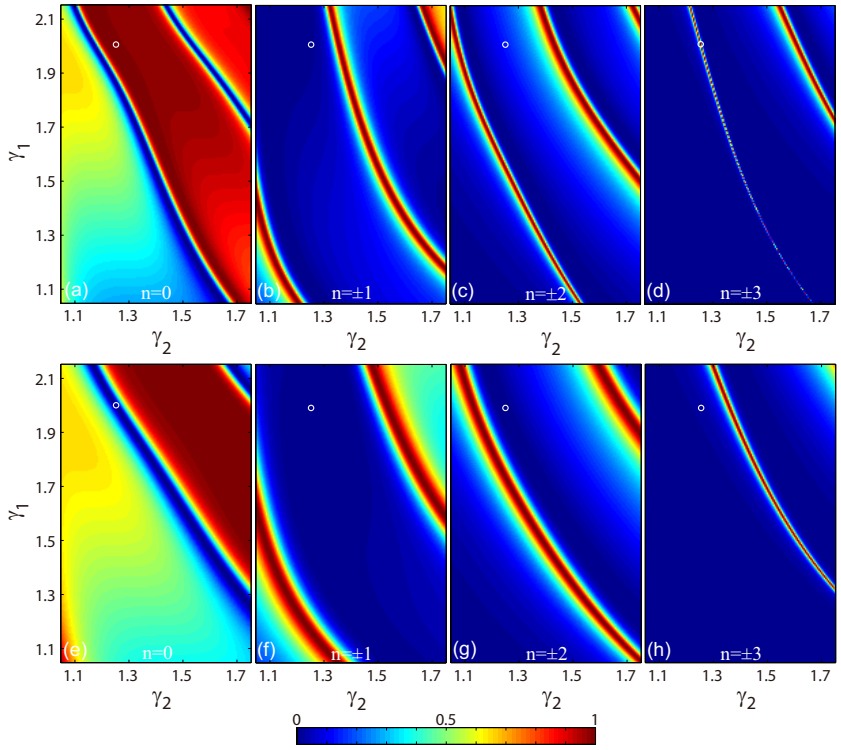

Fig. 5. (a)-(d) The NSCS σ_N for cylindrical structures as in Fig. 1 as a function of $\gamma_1 = \frac{\rho_2}{\rho_1}$ and $\gamma_2 = \frac{\rho_3}{\rho_2}$ for different scattering orders at the wavelength of $\lambda_0 = 4\mu$m for GST in its crystalline phase. The material in the core layer is ZnO, and its radius is $\rho_1 = 480$ nm. The material in the inner shell is TiO_2. (e)-(h) Same as in (a)-(d) except that GST is in its amorphous phase. The three-layer core-shell structure is in the superscattering regime for GST in its crystalline phase, and in the cloaking regime for GST in its amorphous phase at the wavelength of $\lambda_0 = 4\mu$m, when $\gamma_1 = 1.99$ and $\gamma_2 = 1.26$ (white circle).

the resonant scattering regime is broad in the γ_1-γ_2 space for $n = 0$, but narrow for $|n|$ =1, 2, and 3 [Figs. 5(a)-5(d)]. Thus, it is very difficult to achieve overlapping of the dipole ($|n| = 1$), quadrupole ($|n| = 2$), and sextupole ($|n| = 3$) scattering modes. However, superscattering can be realized when there is overlap between the monopole ($n = 0$) and a higher order multipolar mode (dipole, quadrupole, or sextupole). Thus, superscattering occurs when a higher order multipolar scattering mode is on resonance. When the phase-change material GST is in its amorphous phase, the near-zero scattering regime is narrow in the γ_1-γ_2 space for $n = 0$, but quite broad for $|n|$ =1, 2, and 3 [Figs. 5(e)-5(h)]. For the range of parameters shown, the cloaking condition for the proposed moderately small structure can therefore be approximately reduced to $|b_0|^2 = 0$. In other words, cloaking occurs when the amplitude of the monopole scattering coefficient $|b_0|$ is zero. Switching between superscattering and cloaking regimes can be achieved when superscattering for GST in its crystalline phase and cloaking for GST in its amorphous phase occur at the same point in the γ_1-γ_2 space. Figure 5 reveals that the optimized moderately small three-layer core-shell structure is in the superscattering regime for GST in its crystalline phase, and in the cloaking regime for GST in its amorphous phase at the wavelength of $\lambda_0 = 4\mu$m, when $\gamma_1 = 1.99$ and $\gamma_2 = 1.26$ (white circle in Fig. 5). The radius of such a three-layer cylindrical structure is $\rho_3 = \rho_1\gamma_1\gamma_2 = 1023.5$ nm, which is $\sim \frac{\lambda_0}{3.3}$.

To further illustrate the superscattering property of the optimized structure, we show the NSCS

Optical Materials EXPRESS

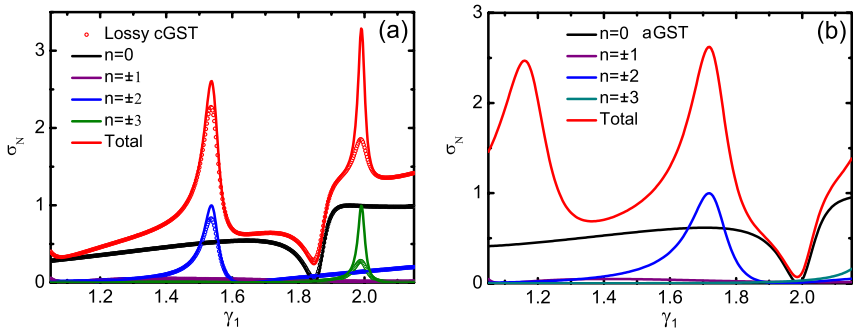

Fig. 6. (a) The NSCS σ_N for cylindrical structures as in Fig. 1 as a function of $\gamma_1 = \frac{\rho_2}{\rho_1}$ with $\gamma_2 = \frac{\rho_3}{\rho_2}$=1.26 at the wavelength of $\lambda_0 = 4\mu$m for GST in its crystalline phase. All other parameters are as in Fig. 5(a). The solid lines and circles correspond to lossless and lossy cGST, respectively. (b) Same as in (a) except that GST is in its amorphous phase.

σ_N for different scattering orders as a function of $\gamma_1 = \frac{\rho_2}{\rho_1}$ with $\gamma_2 = \frac{\rho_3}{\rho_2} = 1.26$ when GST is in its crystalline phase [Fig. 6(a)]. We observe that, when $\gamma_1 = 1.99$, the monopole, quadrupole and sextupole modes overlap very well. In the lossless cGST case, the overall σ_N, which is calculated with full-wave finite-element simulations, can reach ~ 3.29 [Fig. 6(a)]. In the presence of loss, the overall σ_N is reduced to ~ 1.85 [Fig. 6(a)]. Similarly, to further illustrate the cloaking property of the optimized structure, we show the NSCS σ_N for different scattering orders when GST is in its amorphous phase [Fig. 6(b)]. We observe that the overall σ_N can be drastically suppressed for $\gamma_1 = 1.99$, where the monopole mode contribution becomes zero, and the higher order multipolar mode contributions are very small. The corresponding overall σ_N can be as small as ~ 0.067 [Fig. 6(b)]. The contrast ratio τ between the supercattering and cloaking states is $\left|\frac{1.85-0.067}{1.85+0.067}\right| \sim 93\%$.

The switching between cloaking and superscattering regimes at the wavelength of $\lambda_0 = 4\ \mu$m can be observed in the field distributions inside and outside the moderately small core-shell cylindrical structure of Fig. 1 for $\gamma_1 = \frac{\rho_2}{\rho_1} = 1.99$, $\gamma_2 = \frac{\rho_3}{\rho_2} = 1.26$, and $\rho_1 = 480$ nm (Fig. 7). Figure 7(a) shows the magnetic field profile for a bare ZnO core with radius of $\rho_1 = 480$ nm. In this case, the overall σ_N is ~ 0.77. The scattering is dominated by the monopole mode [Fig. 7(b)]. In Figs. 7(c) and 7(d), we show the magnetic field distributions of the optimized three-layer cylindrical structure when GST is in its crystalline phase. When a plane wave is normally incident from the left, the core-shell cylindrical structure induces strong backscattering, and leaves a significant shadow in front of it, where the field strength is reduced [Fig. 7(c)]. The enhanced NSCS (~ 1.85) is 2.4 times larger than that of the bare ZnO core (~ 0.77). We observe that, when $\gamma_1 = 1.99$, the monopole, quadrupole, and sextupole modes overlap very well. The field distribution inside the cylindrical structure is a superposition of the monopole, quadrupole, and sextupole mode fields [Fig. 7(d)], which is consistent with the results associated with superscattering in Fig. 6(a). The monopole modal fields reside mostly in the lossless ZnO core. The strong overlap of the resonant sextupole modal fields with the lossy cGST outer shell leads to a greatly reduced scattering cross section compared to the lossless cGST case [Fig. 6(a)]. Interestingly, even though the material loss in cGST highly affects the sextupole mode, it does not affect much the dipole and quadrupole modes [Fig. 6(a)]. This is due to the weak overlap of the dipole and quadrupole modes with the lossy cGST shell. In addition, the resonant sextupole mode has a higher quality factor than that of the dipole and quadrupole modes [Fig. 6(a)], which results in light being trapped in the structure for a longer duration. This in turn leads to higher power penalty [44, 58]. Similarly, in Figs. 7(e) and 7(f) we show the magnetic field distribution of the optimized three-layer cylindrical structure

Optical Materials EXPRESS

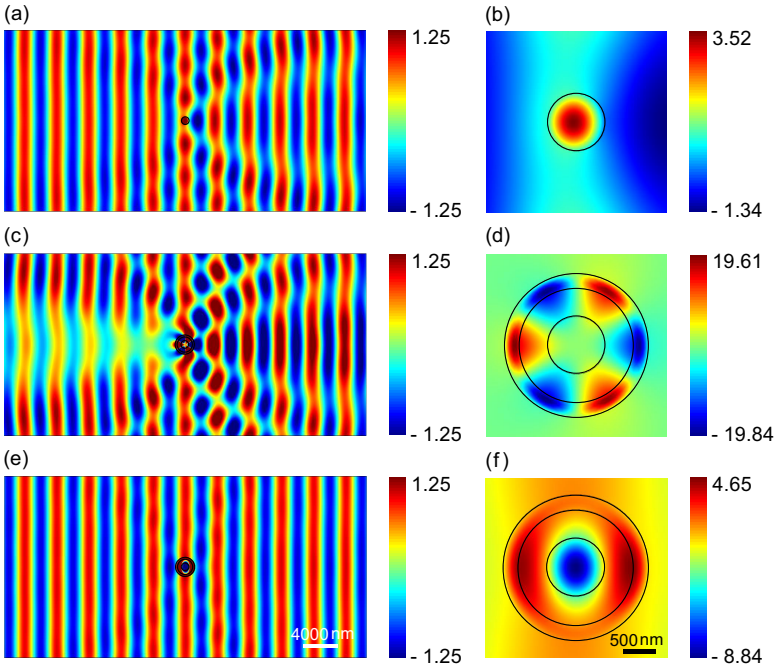

Fig. 7. (a) and (b) Magnetic field amplitude profiles for a bare ZnO core with radius of ρ_1 = 480 nm at the wavelength of λ_0=4 μm, when a plane wave is normally incident from the left. The fields are normalized with respect to the field amplitude of the incident plane wave. (c) and (d) Magnetic field amplitude profiles for the optimized core-shell cylindrical structure of Fig. 1 with GST in its crystalline phase and $\gamma_1 = \frac{\rho_2}{\rho_1} = 1.99$. All other parameters are as in Fig. 6(a). (e) and (f) Same as in (c) and (d) except that GST is in its amorphous phase.

when GST is in its amorphous phase. We observe that in this case there is hardly any scattering. The suppressed NSCS σ_N ($\sim$ 0.067) is 11.5 times smaller than that of the bare ZnO core ($\sim$ 0.77). Two different resonant modes can be observed in the core and shell regions [Fig. 7(f)]. These two excited resonant modes are out-of-phase and compensate each other in the far-field, resulting in scattering cancellation [16].

4. Conclusions

In this paper, we designed subwavelength three-layer core-shell cylindrical structures with the phase-change material GST for switching between the cloaking invisibility and enhanced scattering regimes at the mid-infrared wavelength of λ_0 =4 μm. We used the Mie-Lorenz mode-expansion method and optimized the geometric and material parameters of the structures to achieve the switching. For an electrically small three-layer structure, we optimized the dielectric permittivity of the material in the inner shell and the layer dimensions, to switch between cloaking and resonant scattering by switching the phase-change material GST from its crystalline to its amorphous phase. We found that for the optimized structure the contrast ratio between the cloaking and resonant scattering states is almost unity. For larger, moderately small three-layer structures, we optimized the layer dimensions to minimize the scattering cross section when GST is in its amorphous phase, and maximize the scattering cross section when GST is in its crystalline phase. We found that cloaking occurs when the amplitude of the monopole scattering coefficient is zero, while superscattering occurs when a higher order multipolar scattering mode is on

Optical Materials EXPRESS

resonance. For the optimized structure, the contrast ratio between the cloaking and superscattering states can be as high as ~ 93%. We also confirmed these findings with full-wave finite-element simulations.

As final remarks, we first investigated a two-layer cylindrical structure consisting of a core layer and a GST shell layer. We found that such a two-layer structure cannot achieve the same functionality as the three-layer structure. In other words, the inner shell between the core and the GST outer shell is necessary to achieve switching between cloaking and enhanced scattering regimes. This is due to the fact that for electrically small two-layer cylindrical structures, a shell with negative or near-zero permittivity is necessary to cloak a dielectric core based on scattering cancellation [14, 15]. Thus, an electrically small two-layer structure consisting of a GST shell and a dielectric core cannot be used to realize switching between the cloaking and resonant scattering regimes. We also note that layered core-shell cylindrical nanostructures can be fabricated by chemical vapor deposition and sputter coating [59]. Light scattered from an individual cylindrical nanostructure can be detected using dark-field microscopy [60]. In addition, switching between cloaking and superscattering regimes using phase-change materials could also be generalized to three-dimensional spherical nanostructures [20]. Our results could be potentially important for developing a new generation of dynamically reconfigurable subwavelength optical devices.

Funding

National Natural Science Foundation of China (NSFC) (61605252); Hunan Provincial Natural Science Foundation of China (2017JJ3375); National Key Research and Development Program of China (2016YFC0102401); National Science Foundation (NSF) (1254934).